Behavioral/Cognitive

Reduced Structural Connectivity Between Left Auditory Thalamus and the Motion-Sensitive Planum Temporale in Developmental Dyslexia

Nadja Tschentscher,[1,2] **Anja Ruisinger,**[1] **Helen Blank,**[3] **Begoña Díaz,**[1,4,5] **and Katharina von Kriegstein**[1,6]

[1]Max Planck Institute for Human Cognitive and Brain Sciences, 04103 Leipzig, Germany, [2]Research Unit Biological Psychology, Department of Psychology, Ludwig-Maximilians-Universität Munich, 80802 Munich, Germany, [3]University Medical Center Hamburg-Eppendorf, Center for Experimental Medicine, Institute of Systems Neuroscience, 20246 Hamburg, Germany, [4]Center for Brain and Cognition, Departament de Tecnología de les Comunicacions, Universitat Pompeu Fabra, 08018 Barcelona, Spain, [5]Faculty of Medicine and Health Sciences, Universitat Internacional de Catalunya, 08017 Barcelona, Spain, and [6]Faculty of Psychology, Technische Universität Dresden, Dresden, 01062 Germany

Developmental dyslexia is characterized by the inability to acquire typical reading and writing skills. Dyslexia has been frequently linked to cerebral cortex alterations; however, recent evidence also points toward sensory thalamus dysfunctions: dyslexics showed reduced responses in the left auditory thalamus (medial geniculate body, MGB) during speech processing in contrast to neurotypical readers. In addition, in the visual modality, dyslexics have reduced structural connectivity between the left visual thalamus (lateral geniculate nucleus, LGN) and V5/MT, a cerebral cortex region involved in visual movement processing. Higher LGN-V5/MT connectivity in dyslexics was associated with the faster rapid naming of letters and numbers (RANln), a measure that is highly correlated with reading proficiency. Here, we tested two hypotheses that were directly derived from these previous findings. First, we tested the hypothesis that dyslexics have reduced structural connectivity between the left MGB and the auditory-motion-sensitive part of the left planum temporale (mPT). Second, we hypothesized that the amount of left mPT–MGB connectivity correlates with dyslexics RANln scores. Using diffusion tensor imaging-based probabilistic tracking, we show that male adults with developmental dyslexia have reduced structural connectivity between the left MGB and the left mPT, confirming the first hypothesis. Stronger left mPT–MGB connectivity was not associated with faster RANln scores in dyslexics, but was in neurotypical readers. Our findings provide the first evidence that reduced cortico-thalamic connectivity in the auditory modality is a feature of developmental dyslexia and it may also affect reading-related cognitive abilities in neurotypical readers.

Key words: developmental dyslexia; DWI; medial geniculate body (MGB); planum temporale (PT); primary auditory cortex (A1); RAN

Significance Statement

Developmental dyslexia is one of the most widespread learning disabilities. Although previous neuroimaging research mainly focused on pathomechanisms of dyslexia at the cerebral cortex level, several lines of evidence suggest an atypical functioning of subcortical sensory structures. By means of diffusion tensor imaging, we here show that dyslexic male adults have reduced white matter connectivity in a cortico-thalamic auditory pathway between the left auditory motion-sensitive planum temporale and the left medial geniculate body. Connectivity strength of this pathway was associated with measures of reading fluency in neurotypical readers. This is novel evidence on the neurocognitive correlates of reading proficiency, highlighting the importance of cortico-subcortical interactions between regions involved in the processing of spectrotemporally complex sound.

Introduction

Developmental dyslexia is characterized by the inability to develop neurotypical levels of reading and writing skills despite unimpaired fluid intelligence and adequate educational opportunities (Peterson and Pennington, 2012, 2015). It is the most

Received June 7, 2018; revised Nov. 2, 2018; accepted Nov. 25, 2018.

Author contributions: N.T. and K.v.K. designed research; B.D. performed research; N.T. analysed data; A.R. and H.B. contributed to data analysis; N.T. and K.v.K. wrote the paper; N.T., H.B., and K.v.K. edited the paper.

This work was supported by a Max Planck Research Group Grant and the European Research Council (ERC-Consolidator Grant SENSOCOM, 647051) to K.v.K. We thank our participants for their time and effort to participate in this study. We thank Domenica Wilfling, Elisabeth Wladimirow, and Florian Hintz for providing the structural MRI data and the dyslexia diagnostic scores and Alfred Anwander and Christa Müller-Axt for helpful advice on our tracking analysis protocols.

The authors declare no competing financial interests.

Correspondence should be addressed to Nadja Tschentscher at tschentscher@cbs.mpg.de.

https://doi.org/10.1523/JNEUROSCI.1435-18.2018

 0270-6474/19/391720-13$15.00/0

widespread learning disability, with a prevalence of 5–10% in children, and often leads to severe emotional and social difficulties (Carroll and Iles, 2006).

Most neuroscientific research has investigated pathomechanisms of developmental dyslexia, which we will refer to as dyslexia in the following, at the cerebral cortex level (for review, see Vandermosten et al., 2012). However, there is also evidence of dyslexia-related alterations in subcortical regions in the left auditory thalamus (medial geniculate body, MGB) (Díaz et al., 2012) and auditory brainstem (Chandrasekaran et al., 2009; Chandrasekaran and Kraus, 2010). Examinations of postmortem brains showed histological changes in the left MGB of several patients with dyslexia (Galaburda et al., 1994; cf. Stein, 2001). It is a long-standing but never tested hypothesis that these changes are associated with altered fiber connectivity between the left MGB and those cerebral cortex areas that show alterations in dyslexia (Galaburda et al., 1994).

Here, we tested the specific hypothesis that dyslexics have reduced structural connectivity between the left MGB and those parts of the left auditory association cortex (planum temporale, PT) (Westbury et al., 1999) that are involved in the processing of auditory motion; we will abbreviate this region mPT (motion-sensitive planum temporale). Our focus on the mPT rests on two strands of evidence. First, the PT has been implicated in dyslexia as part of a left-hemispheric dysfunctional language system (for review, see Shapleske et al., 1999; Altarelli et al., 2014). Structural MRI analyses showed atypical interhemispheric symmetry of PT volumes (Altarelli et al., 2014) and postmortem brain analyses reported histological alterations in the PT of dyslexics (Galaburda et al., 1985; Humphreys et al., 1990). Critically, those histological alterations have not been reported for primary auditory (A1) cortices (for review, see Eckert, 2004). Second, in the visual modality, reduced left-hemispheric structural connectivity has been observed between the visual thalamus (lateral geniculate nucleus, LGN) and middle temporal area V5/MT, whereas connectivity between the LGN and the primary visual cortex (V1) was at a neurotypical level (Müller-Axt et al., 2017). V5/MT is an extrastriate visual cortex region implicated in visual motion processing (Britten et al., 1992; Zeki, 2015). The most functionally equivalent region to V5/MT in the auditory modality is the PT, which houses a key region for auditory motion processing (Warren et al., 2002; Alink et al., 2012); this is the region that we here call mPT. The PT is tonotopically organized (Langers, 2014) and animal tracing studies (Bajo et al., 1995; Winer et al., 2001; Lee and Winer, 2008) reported direct fiber connectivity between tonotopically organized regions (Langers and van Dijk, 2012; Langers, 2014) and the MGB.

Using diffusion tensor imaging (DTI)-based probabilistic tractography, we here compared male adults with dyslexia ($n = 12$) with matched neurotypicals ($n = 12$). First, we tested whether connectivity strength between the left mPT and the left MGB is weaker in dyslexics than in neurotypicals. Second, we expected that connectivity strength between the left mPT and the left MGB in dyslexics correlates with the rapid automatized naming of letters and numbers (RANln), and with reading comprehension. The RANln predicts reading abilities (Semrud-Clikeman et al., 2000; Miller et al., 2006; cf. Lervåg and Hulme, 2009; for review, see Norton and Wolf, 2012). In dyslexic adults, lower RANln and reading comprehension scores were associated with reduced fMRI responses in the left MGB (Díaz et al., 2012). The RANln also correlated with connectivity strength in the left LGN–V5/MT pathway (Müller-Axt et al., 2017). We tested the specificity of the expected left mPT–MGB connectivity reduction by assessing the right-hemispheric white matter connectivity between MGB and mPT and MGB's connectivity with A1. We also explored MGB's connectivity with the immediately preceding nucleus in the auditory brainstem, the inferior colliculus (IC).

Table 1. Social demographic and cognitive measures (mean ± SD) of 12 male dyslexics and 12 male neurotypical participants

	Neurotypical group ($n = 12$)	Dyslexia group ($n = 12$)	Two-sample t test, neurotypicals − dyslexics
Demographic data			
Age in years	23.7 ± 2.6	24.2 ± 2.3	NS
Handedness	right = 11, left = 1	right = 10, left = 2	—
Education	11 undergrad. students, 1 high school diploma	12 undergrad. students	—
Diagnostic tests			
Nonverbal IQ (Raven matrices)	110.8 ± 12.8	101 ± 13.6	NS
Spelling	102.8 ± 5.6	83.1 ± 7.6	$t_{(22)} = 7.2, p < 0.001$
Reading speed	58.3 ± 9.1	42.6 ± 6.5	$t_{(22)} = 4.9, p < 0.001$
Reading comprehension	62.9 ± 7.7	47.4 ± 4.2	$t_{(22)} = 6.1, p < 0.001$
RAN numbers time (ms)	16.8 ± 2.4	21.2 ± 6.1	$t_{(22)} = 2.3, p < 0.05$
RAN numbers errors (%)	0.8 ± 1.3	0.2 ± 0.6	NS
RAN letters time (ms)	16.4 ± 2.6	20.3 ± 3.5	$t_{(22)} = 3.1, p < 0.01$
RAN letters errors (%)	0.3 ± 1.2	0.3 ± 0.8	NS

The Raven matrices test (mean = 100, SD = 15), spelling test (mean = 100, SD = 10), and reading speed and comprehension tests (mean = 50, SD = 10) are all based on standard scores.
NS, Not significant.

Materials and Methods

Participants

Data from two groups of healthy male native German speakers without any history of neurological or psychiatric diseases were analyzed. The group of subjects with reading and writing impairments (dyslexia group) included 12 participants, of which six had been formally diagnosed with dyslexia, whereas the other six reported severe reading and spelling difficulties since childhood. The neurotypical group included 12 participants with average reading and spelling abilities and was matched in age, sex, educational level, handedness, and nonverbal IQ (Raven, 1998) to the dyslexia group. For the same participant groups, a dyslexia-specific reduction in left MGB responses during speech processing has been reported (Díaz et al., 2012), as well as a reduction in structural connectivity between the left LGN and V5/MT (Müller-Axt et al., 2017).

A formal behavioral assessment on reading speed and comprehension (Schneider et al., 2007), spelling (Kersting and Althoff, 2004), and skills of rapid automatized naming (i.e., RANln) (Denckla and Rudel, 1976) confirmed the group assignments: lower scores on spelling, reading speed, and comprehension were observed in the dyslexia group, as well as longer reaction times in RANln (Table 1). A median-split analysis based on the average scores of spelling, reading speed, and reading comprehension revealed the same group assignments as defined *a priori* based on clinical diagnoses of dyslexia and self-reports of participants on their reading and spelling abilities. The diagnostic test scores and social demographic variables are summarized in Table 1. Written informed consent was obtained from all participants before data acquisition. The study was approved by the ethics committee of the Medical Faculty, University of Leipzig, Germany.

Data acquisition of diffusion-weighted and anatomical T1-weighted images

We acquired diffusion-weighted images (dMRI) on a 3 tesla Magnetom Tim Trio MRI system with a 32-channel head coil (Siemens) using a twice-refocused spin-echo echoplanar imaging (EPI) sequence (TE = 100 ms, TR = 12.9 s, FOV = 220 × 220 mm^2, voxel size = 1.72 × 1.72 × 1.7 mm^3). Eighty-eight axial slices were obtained, covering the whole brain without interslice gap. Diffusion weighting was isotropically distributed along 60 diffusion-encoding gradient directions with a b-value of 1000 s/mm^2. For offline motion correction, seven interspersed anatomical reference images were acquired without diffusion weighting (b-

value = 0 s/mm^2): one in the beginning and one after each of the blocks of 10 diffusion-weighted images. Fat saturation was applied using a spectral saturation pulse. Generalized autocalibrating partially parallel acquisitions (GRAPPA; Griswold et al., 2002) was used with an acceleration factor of 2, as well as partial Fourier imaging of 6/8 to accelerate the dMRI acquisition. The dMRI sequence took ~16 min. A T1-weighted structural 3D image was acquired as anatomical reference on the same MRI system (MPRAGE, TE = 3.46 ms, TR = 1300 ms, TI = 650 ms, flip angle = 10°, 1 mm isotropic resolution, two averages).

Preprocessing of dMRI data

FSL (FMRIB Software Library, University of Oxford, http://www.fmrib.ox.ac.uk/fsl) was used to estimate motion correction parameters for the dMRI data based on the seven reference images without diffusion-weighting and rigid-body registration (Jenkinson et al., 2002). Motion correction parameters were interpolated for all 67 volumes and combined with a global registration to the T1 anatomy (in AC/PC space) using rigid-body registration. The estimated motion correction parameters were then used to correct the gradient directions of each dMRI volume. The registered dMRI volumes were sampled with an isotropic voxel resolution of 1.72 mm and the background was masked with the skull-stripped T1 image. A diffusion tensor was fitted to each voxel and fractional anisotropy (FA) maps were computed (Basser et al., 1994; Basser and Pierpaoli, 1996).

Functional localizer for ROI definition

To localize ROIs in the auditory pathway, we used a functional localizer acquired on the same participant sample (Díaz et al., 2012). Participants listened passively to blocks of auditory sentences that were separated by silence. The stimuli consisted of 40 five-word sentences that were semantically neutral (e.g., "Der Junge trägt einen Koffer," meaning "The boy carries a suitcase") and syntactically similar (i.e., subject–verb–object) recorded from a 22-year-old male German speaker. fMRI data were acquired on a 3 T Magnetom TIM Trio (Siemens) by using a 32-channel head coil (Siemens). A gradient-echo EPI sequence was applied (echo time = 30 ms, flip angle = 90°, acquisition bandwidth = 116 kHz, slice thickness = 2 mm, interslice gap = 1 mm, 42 slices, axial and ascending acquisition starting at the pontomedullary junction). A sparse sampling imaging protocol with cardiac gating was applied, which is thought to reduce the artifacts caused by the pulsatile motion of the brainstem (Hall et al., 1999; Thompson et al., 2006). The 82 brain volumes of each participant were analyzed with SPM8 (https://www.fil.ion.ucl.ac.uk/spm/) and MATLAB version 7.10 (R2010a; The MathWorks). Scans were realigned, unwarped, coregistered to the individual anatomical images, and normalized to Montreal Neurological Institute (MNI) standard stereotactic space. Images were spatially smoothed with a Gaussian smoothing kernel of 4 mm full-width at half maximum for subcortical structures and a smoothing kernel of 8 mm for cortical structures. A general linear model was applied using a boxcar function convolved with a synthetic hemodynamic response function to model the metabolic signal.

Definition of subcortical ROIs

Subcortical ROIs were based on group-level peak coordinates from the functional localizer contrast "Sentences - Silence". Compared with the LGN (Müller-Axt et al., 2017), it is difficult to delineate the MGB on structural images (Devlin et al., 2006; Jiang et al., 2013; Tourdias et al., 2014). Devlin et al. (2006) have identified MGBs at the single-subject level based on proton density (PD) images and a DTI approach and Javad et al. (2014) defined MGBs on T1-weighted images; however, there are so far no indications that these procedures yield more reliable information than a functional approach on the single-participant level or with random-effects group analyses with commonly used statistical thresholds (Jiang et al., 2013). Because localization at a single-subject level was not possible in all participants in our study, we used an ROI based on the sample specific random effects coordinate obtained for the contrast "Sentences – Silence" (Díaz et al., 2012).

For the MGB, a spherical mask of 4 mm radius was defined around the statistical maxima present in the anatomical location of the left and right MGB (left [−15, −28, −5], and right [12, −28, −8] in MNI space). These coordinates have been previously used in fMRI analyses on the top-down modulation of the MGB in the same dyslexia sample (Díaz et al., 2012). The gray matter proportion of the mask matched the size of the reported gray matter volume of the MGB in previous *in vivo* structural MRI as well as postmortem analyses (Rademacher et al., 2002; Devlin et al., 2006; Javad et al., 2014), which reported mean left MGB volumes between 38 mm^3 and 123 mm^3 (see Fig. 1 for masks and functional localizer clusters and Table 2 for subcortical ROI volumes).

The MGB statistical maxima in the functional localizer were not exactly symmetric across hemispheres (left [−15, −28, −5], and right [12, −28, −8] in MNI space). Similar asymmetries in the *x* and *z* direction have been previously observed by other neuroimaging studies (Devlin et al. (2006), left MGB [−14, −25, −6], right MGB [13, −25, −7]; Jiang et al. (2013), left MGB study 1 [−15, −25, −7], left MGB study 2 [−16, −26, −6], right MGB study 1 [13, −25, −6], right MGB study 2 [13, −26, −6]; Moerel et al. (2015), left MGB [−16, −23, −9], right MGB [14, −23, −9]).

Linear and nonlinear registration was performed in FSL using the default parameters to bring the MGB masks into diffusion space. A reasonable placement of the masks on the single-subject level was evaluated by visual inspection. To provide an example of this process, Figure 2 shows the placement of the MGB masks on the single-subject T1 images of six randomly chosen subjects within the groups of dyslexics and neurotypicals. To extract gray and white matter, a binarized FA < 0.2 image of each participant was used in diffusion space (see Table 2 for gray and white matter ROI volumes).

For the IC, a spherical mask with a radius of 3 mm was created around peak coordinates from the functional localizer (left [−6, −34, −8], and right [6, −37, −5] in MNI space; Fig. 3, yellow). The gray matter part of the mask matched the size of previously reported gray matter volumes of the IC (Sabanciogullari et al., 2013; Table 2). Linear and nonlinear registration was performed in FSL using the default parameters to bring the IC masks into diffusion space. Again, a binarized FA < 0.2 image of each participant was used to extract gray and white matter masks in diffusion space (see Table 2 for gray and white matter ROI volumes). Also for the IC, statistical maxima were not entirely symmetric (left [−6, −34, −8], and right [6, −37, −5] in MNI space). Asymmetries in IC coordinates have been observed in previous fMRI studies; however, whether this is a general feature of IC BOLD responses is unclear because IC coordinates are often not reported (Melcher et al., 2000; De Martino et al., 2013; Ress and Chandrasekaran, 2013). There was also an alternative coordinate for the left IC at [−3, −37, −8] in the functional localizer contrast "Sentences - Silence". This coordinate had a slightly lower statistic ($Z = 4.25$). We chose to report the results for [−6, −34, −8] due to its higher *Z* score ($Z = 4.35$). However, we additionally performed analyses with ROIs based on the alternative coordinate [−3, −37, −8].

Definition of cerebral cortex ROIs

The cerebral cortex ROIs in A1 and mPT were created in two steps. First, we created spherical masks around a functional MRI coordinate (for details, see below). Second, these spherical masks were intersected with thresholded probabilistic volume based atlas masks to ensure that the ROIs did not exceed the anatomically defined regional boundaries of A1 and PT, respectively. For the A1 ROIs, the peak coordinates for the spherical masks were extracted from the functional localizer contrast "Sentences – Silence" in the left [−51, −16, 4] and right [42, −22, 7] hemispheres in MNI space (Fig. 1). These coordinates have been used in previous fMRI analyses on the same subject sample (Díaz et al., 2012). To define the mPT, we used the coordinates reported by Alink et al. (2012) for the left [−53, −31, 12] and right [54, −29, 14] hemisphere in MNI space, respectively. We chose these coordinates for the intersections with volume-based atlas masks, because Alink et al. (2012) successfully decoded the direction of moving sounds from fMRI response patterns of bilateral PT volumes centered at these coordinates.

We created spherical masks (radius = 8 mm) around A1 and mPT peak coordinates. The A1 sphere was intersected with the thresholded probabilistic TE1.0 atlas mask from the Juelich histological atlas (Eickhoff et al., 2005). The mPT sphere was intersected with the PT mask from the Harvard–Oxford atlas (Desikan et al., 2006). We used these two different atlases, because the Juelich atlas does not include the PT and the

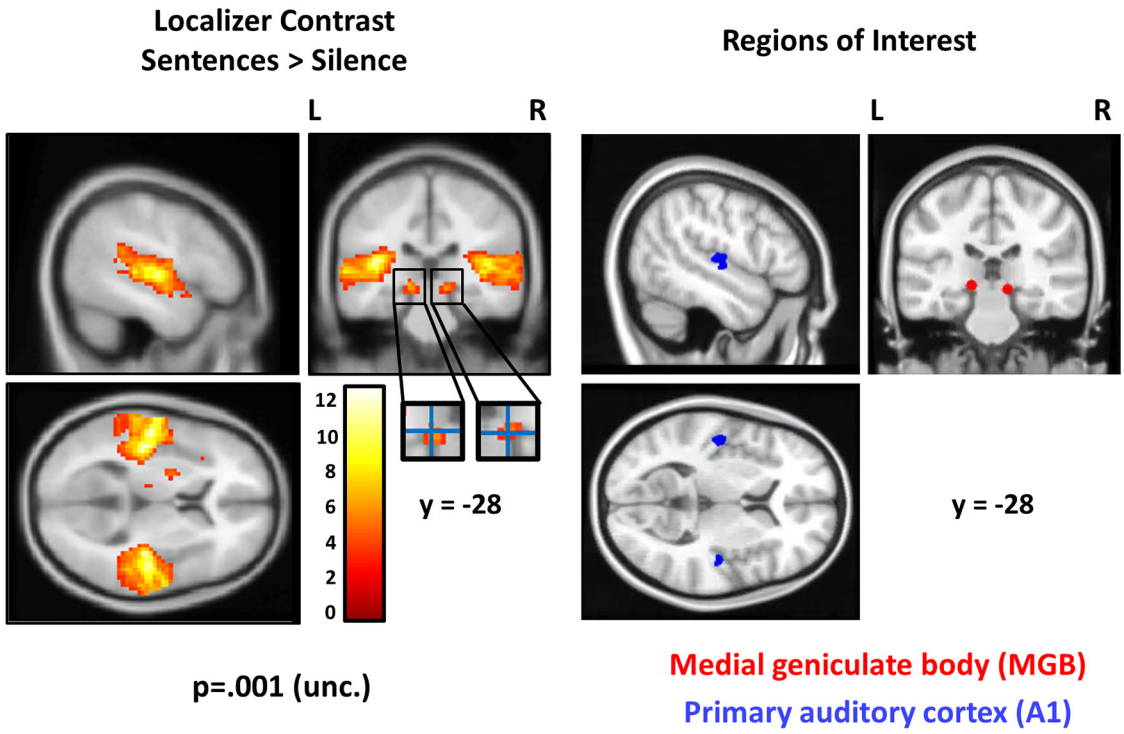

Figure 1. The left side of the figure displays the statistical parametrical map of the localizer contrast "Sentences - Silence". The color bar represents *t*-values. The crosshair over the zoomed-in medial geniculate body responses indicates the statistic peak location from the localizer contrast "Sentences – Silence" used for definition of ROIs. The right side shows the ROIs centered at the statistic peak location of the localizer contrast "Sentences – Silence". The maps and ROIs are superimposed on the same section of the MNI152 structural T1 volume.

Table 2. Size of subcortical ROIs in diffusion space

ROI volumes (mm^3), mean ± SD	Neurotypical group ($n = 12$)	Dyslexia group ($n = 12$)	Two-sample *t* test, neurotypicals − dyslexics
Left MGB			
Grey and white matter	347.86 ± 32.30	364.20 ± 33.32	$t_{(22)} = -1.22, p = 0.235$
Grey matter	70.82 ± 34.07	117.34 ± 30.50	$t_{(22)} = -3.52, p = 0.001$**
White matter	277.02 ± 59.87	246.85 ± 44.64	$t_{(22)} = 1.39, p = 0.175$
Right MGB			
Grey and white matter	349.53 ± 53.97	348.69 ± 24.29	$t_{(22)} = 0.049, p = 0.961$
Grey matter	115.25 ± 47.44	151.71 ± 35.80	$t_{(22)} = -2.12, p = 0.045$*
White matter	234.28 ± 52.76	196.98 ± 27.86	$t_{(22)} = 2.16, p = 0.041$*
Left IC			
Grey and white matter	153.39 ± 26.57	172.25 ± 25.56	$t_{(22)} = -1.77, p = 0.090$
Grey matter	85.50 ± 28.21	103.92 ± 22.52	$t_{(22)} = -1.76, p = 0.090$
White matter	67.89 ± 19.48	68.31 ± 14.46	$t_{(22)} = -0.05, p = 0.952$
Right IC			
Grey and white matter	138.72 ± 31.11	163.45 ± 26.39	$t_{(22)} = -2.10, p = 0.047$*
Grey matter	119.85 ± 27.45	138.30 ± 35.00	$t_{(22)} = -1.43, p = 0.165$
White matter	18.86 ± 11.95	25.15 ± 14.05	$t_{(22)} = -1.18, p = 0.250$

Spherical masks were defined around the statistical maxima of the functional localizer in the anatomical locations of the left and right MGB (left [−15, −28, −5], and right [12, −28, −8] in MNI space) and left and right IC (left [−6, −34, −8] and right [6, −37, −5] in MNI space), respectively. *$p < 0.05$, **$p < 0.01$.

Havard–Oxford atlas does not include a mask solely covering A1. Both atlases are implemented in FSL in MNI standard space with a voxel resolution of 1 mm^3. Mask volumes from probabilistic atlases were thresholded to the size of the approximate volumes of A1 (Rademacher et al., 2001; Artacho-Pérula et al., 2004) and the PT (Hirayasu et al., 2000; Ratnanather et al., 2013), as known from postmortem studies and MRI segmentations. Intersections between these masks and the spherical volumes were calculated in FSL (see Fig. 3 for masks and Table 3 for ROI volumes). Linear and nonlinear registration was performed in FSL using the default parameters to bring the masks into diffusion space. A binarized FA < 0.2 image of each subject was used to extract gray and white matter masks in diffusion space (see Table 3 for gray and white matter ROI volumes).

Probabilistic tractography

Anatomical connectivity was estimated using FDT (FMRIB's Diffusion Toolbox; https://fsl.fmrib.ox.ac.uk/fsl/fslwiki/FDT). Voxelwise estimates of the fiber orientation distribution were computed using BEDPOSTX (Bayesian Estimation of Diffusion Parameters Obtained using Sampling Techniques) (Behrens et al., 2007). The distribution of up to two fiber orientations at each voxel was estimated based on the b-value and resolution of the dMRI data (Behrens et al., 2003). Probabilistic tractography was performed in native diffusion space using the PROBTRACKX2 module to estimate the strength and the most likely location of a pathway between the respective seed and target areas. Probabilistic tracking from A1 and mPT volumes to the MGB, as well as between the MGB and the IC, was run for each hemisphere separately.

In cortico-subcortical tracking analyses, cortical regions (A1 and mPT) were set as seed masks. The left MGB was defined as waypoint and termination mask so that only tracks that reached the MGB were counted, as well as those that terminated in the MGB (i.e., did not go further). We only computed the tractography from the cerebral cortex ROIs to the MGB to ensure that possible nondominant cortico-subcortical connectivity was detected as well, which might be missed by the algorithm when seeding in the MGB. Seeding in regions with relatively low anisotropy such as the MGB may lead to large uncertainty in fiber orientation (Jones, 2010).

Modified Euler streamlining was applied, but all other default parameters were kept. All analyses were done separately for each pair of seed and target region within each hemisphere. Tractography results were considered reliable when at least 10 of the generated sample streamlines reached the target, a threshold that has been used in previous probabilistic tracking studies (Heiervang et al., 2006; Makuuchi et al., 2009; cf. Blank et al., 2011; Müller-Axt et al., 2017). Less reliable connections were excluded from statistical analyses. Because the number of estimated streamlines for each pair of seed and target region is highly determined by the size of the seed, we corrected for the number of voxels in the respective seed mask. A connectivity index was calculated that reflects the connection strength between pairs of seed and target regions: the number of streamlines from a given seed that reach the target (*waytotals*) was log-

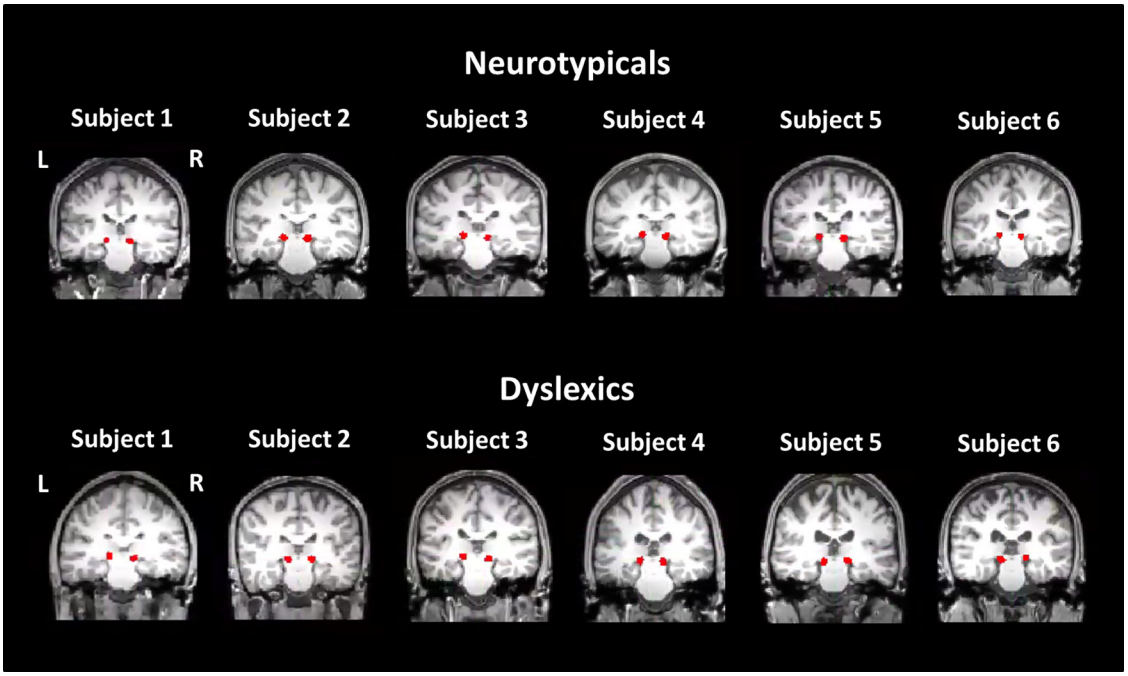

Figure 2. Localization of the MGB masks on the individual subject T1 brain presented for six randomly chosen dyslexic and neurotypical participants.

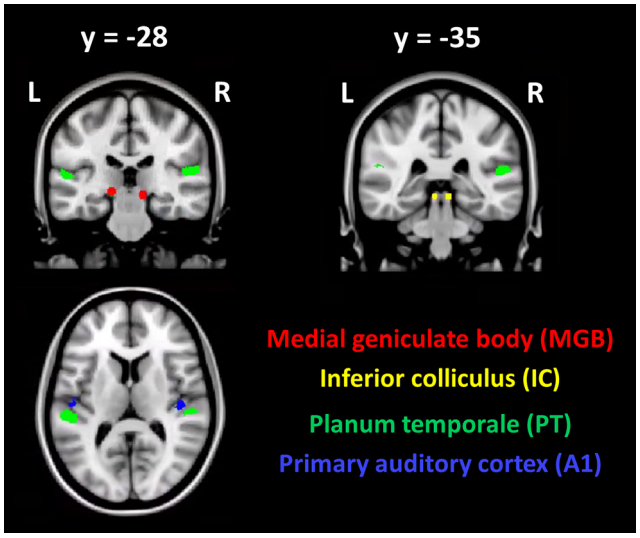

Figure 3. ROIs in MNI standard space superimposed on sections of the MNI152 structural T1 volume.

Table 3. Size of cortical ROIs in diffusion space

ROI volumes (mm^3), mean ± SD	Neurotypical group ($n = 12$)	Dyslexia group ($n = 12$)	Two-sample *t* test, neurotypicals − dyslexics
Left mPT			
Grey and white matter	1369.22 ± 257.36	1147.93 ± 201.34	$t_{(22)} = 2.34, p = 0.028$*
Grey matter	959.33 ± 235.43	804.68 ± 126.19	$t_{(22)} = 2.00, p = 0.057$
White matter	282.47 ± 95.22	232.60 ± 125.52	$t_{(22)} = 1.09, p = 0.284$
Right mPT			
Grey and white matter	1246.42 ± 158.86	1167.21 ± 185.40	$t_{(22)} = 1.12, p = 0.273$
Grey matter	856.23 ± 135.27	722.95 ± 144.25	$t_{(22)} = 2.33, p = 0.029$*
White matter	194.04 ± 104.93	252.30 ± 87.55	$t_{(22)} = -1.47, p = 0.153$
Left A1			
Grey and white matter	760.67 ± 103.36	700.32 ± 128.31	$t_{(22)} = 1.26, p = 0.217$
Grey matter	510.89 ± 93.01	464.37 ± 85.16	$t_{(22)} = 1.27, p = 0.214$
White matter	249.78 ± 111.84	235.95 ± 66.14	$t_{(22)} = 0.368, p = 0.715$
Right A1			
Grey and white matter	594.29 ± 136.80	527.23 ± 111.20	$t_{(22)} = 1.31, p = 0.201$
Grey matter	453.05 ± 99.00	375.93 ± 96.52	$t_{(22)} = 1.93, p = 0.066$
White matter	141.23 ± 68.77	151.29 ± 50.17	$t_{(22)} = -0.409, p = 0.686$

Peak coordinates within the A1 (left [−51, −16, 4], and right [42, −22, 7] in MNI space) and PT (left [−53, −31, 12], and right [54, −29, 14] in MNI space) were intersected with thresholded atlas masks from the Juelich histological atlas (Eickhoff et al., 2005) and the Harvard–Oxford atlas (Desikan et al., 2006), respectively. *$p < 0.05$.

transformed and divided by the log-transformed product of the generated sample streamlines in each seed voxel (5000) and the number of voxels in the respective seed mask (V_{seed}) as follows:

$$Connectivity\ \text{Index} = \frac{\log\,(waytotal)}{\log\,(5000 * V_{seed})},$$

The log transformation increased the likelihood of gaining a normality distribution, which was tested before application of parametric statistics using the Shapiro–Wilk test (Royston, 1992).

For visualization purposes (in Figs. 4, 6, and 7), the output images of the probabilistic tractography for each connection and subject were normalized by logarithmic transformation and then divided by the logarithm (log) of the total number of generated streamlines in each seed mask. This was the same normalization procedure as described for computation of the connectivity index. The normalized tracts were transformed into MNI standard space, averaged within groups of dyslexics and neurotypicals, and thresholded to the same minimum value.

Statistical analyses

Group differences in connectivity strength. Statistical analyses were run in MATLAB version R2016b. Individual participants' connections were considered as inconsistent if the connectivity index exceeded the threshold of 2.5 SDs above or below the group mean of their respective group. After exclusion of these outliers, connectivity indices were subjected to random-effects analyses. A two-sample *t* test was used to test our first hypothesis that there is reduced connectivity in the left mPT–MGB connection in dyslexics compared with neurotypicals.

To test the specificity of the putative group differences in the left mPT–MGB connection, we performed two mixed-effects ANOVAs. First, we tested whether group differences in the mPT–MGB connection were present in the left mPT–MGB pathway, but not in the right mPT–MGB pathway. To do that, we performed a 2 × 2 mixed-effects ANOVA with the factors "hemisphere" (left vs right) and "group" (neurotypicals

vs dyslexics). There were two reasons that we expected group differences in the left mPT–MGB pathway only: alterated BOLD responses of dyslexics in a speech processing task were restricted to the left MGB (Díaz et al., 2012) and postmortem analyses revealed histological alterations in the left MGB, whereas no such findings were reported for the right hemisphere (Galaburda et al., 1994; cf. Stein, 2001). In the second mixed-effects ANOVA with the factors "seed region" (left A1 vs left mPT) and "group" (neurotypicals vs dyslexics), we tested whether the putative group differences were present in the mPT–MGB connection but not in the A1–MGB connection. The left A1–MGB connection was also tested for significant group differences and putative hemispheric differences in the A1–MGB connection were assessed in an 2 × 2 mixed-effects ANOVA with the factors "hemisphere" (left vs right) and "group" (neurotypicals vs dyslexics). We did not expect any dyslexia specific abnormalities in the A1–MGB connection because A1, as opposed to PT, did not reveal histological alterations in postmortem studies (for review, see Eckert, 2004) and, in the visual system, no reduction in structural connectivity was observed in the LGN–V1 pathway (Müller-Axt et al., 2017).

We also performed the following control and exploratory analyses. First, we analyzed the left mPT–MGB connection via A1 by performing an ANOVA with the factors "group" (neurotypicals vs dyslexics) and "track" (left mPT–MGB vs left mPT–MGB-via-A1). This was to rule out that a putative left mPT–MGB connectivity reduction in dyslexics is caused by alterations in left A1–MGB pathway. Second, we assessed group effects in the MGB–IC connection by performing two-sample *t* tests as well as an ANOVA with the factors "hemisphere" (left vs right) and "group" (neurotypicals vs dyslexics). This was to address the finding of several studies associating dyslexia with alterations of auditory brainstem structures (Chandrasekaran et al., 2009; Chandrasekaran and Kraus, 2010).

We first performed all analyses with ROIs that contained both gray and white matter voxels. The extension of gray matter regions to the surrounding white matter clusters is common practice in DTI-based probabilistic tractography analyses (Park et al., 2004; Soares et al., 2013; Thomas et al., 2014). Because gray matter and cerebrospinal fluid have low anisotropy, tracking only from and to gray matter voxels (instead of white matter voxels adjacent to the gray matter ROI) yields less robust probabilistic tractography results (Jones et al., 2013). Importantly, no group effect in the size of MGB volumes was observed for ROIs that contained both gray and white matter voxels (Table 2). Group effects in the volumes of seed masks (i.e., mPT; Table 3) were corrected within the tractography analysis pipeline by accounting for the number of voxels in the respective seed mask (i.e., the connectivity index was calculated in a way that the number of streamlines from a given seed that reached the target was corrected by the number of voxels in the respective seed mask, see "Probabilistic tractography" section). In addition, we performed tractography analyses with the white matter ROIs (cf. Anwander et al., 2007; Blank et al., 2011) for which no group differences were found in left-hemispheric subcortical ROIs (Table 2) and cerebral cortex ROIs (Table 3). We did not further analyze tractography results from gray matter ROIs (Behrens and Johansen-Berg, 2005) because the estimated tracks could not be considered reliable (i.e., there were not >10 streamlines reaching the target ROI): two neurotypicals and eight dyslexics did not show reliable estimates for the connection left mPT–MGB and four dyslexics did not show reliable estimates for the connection left A1–MGB.

Effect sizes for the analyses were calculated using η^2 (Cohen, 1973) for ANOVAs and Cohen's *d* (Cohen, 1988) for two-sample *t* tests.

Correlation of connectivity measures with behavioral scores. To test our second hypothesis, that lower reading skills in dyslexics are associated with weaker left mPT–MGB connectivity strength, we correlated the respective connectivity measure with two behavioral scores: the RANln and reading comprehension. The RAN is a measure of reading fluency (for review, see Norton and Wolf, 2012), which previously correlated with atypical fMRI responses in the left MGB of dyslexics (Díaz et al., 2012), as well as cortico-subcortical structural connectivity strength in the visual pathway (Müller-Axt et al., 2017). Lower reading comprehension scores in dyslexics were also associated with atypical left MGB BOLD signal changes (Díaz et al., 2012). We hypothesized that weaker left mPT–MGB connectivity is associated with lower RANln and reading comprehension scores and Bonferroni corrected for the four conducted *t* tests on the Pearson's correlations as follows: the correlations between the two behavioral scores of interest and the connectivity indices from the two analyses with ROIs containing gray and white matter voxels and ROIs containing white matter voxels only. We report 95% confidence intervals from bootstrapping with 1000 sampling rounds together with parametric statistical tests.

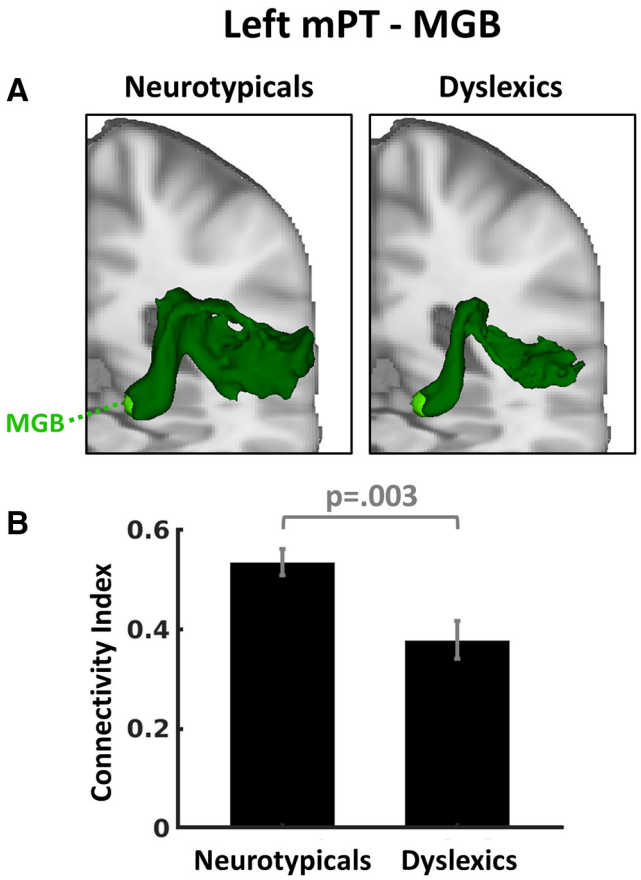

Figure 4. ***A***, Averaged probabilistic white matter connectivity for neurotypicals and dyslexics between the left mPT and the left MGB (green). The log-normalized and averaged tracks are presented in MNI standard space and thresholded to the same minimum value of 0.08. ***B***, Mean connectivity strength of the left mPT–MGB connection for neurotypicals and dyslexics. Error bars indicate ± 1 SEM.

Results

Left mPT–MGB connectivity is reduced in dyslexics compared with neurotypicals

The connection between the left mPT and the left MGB could be reliably estimated in all ($N = 24$) participants for ROIs, including white and gray matter, with at least 10 of the generated sample streamlines reaching the target mask. One neurotypical participant was excluded due to a lower-bound outlier in the left mPT–MGB connection.

To test our hypothesis that dyslexia is associated with reduced connectivity between left mPT and left MGB, we analyzed the differences in left mPT–MGB connectivity indices between dyslexic and neurotypical participants by means of a two-sample *t* test. Consistent with our hypothesis, there were higher connectivity indices for neurotypicals than dyslexics in the left mPT–MGB connection ($t_{(21)} = 3.27$, $p = 0.003$, $d = 1.378$; Fig. 4). To control for potential biases due to group differences in the mPT volumes (Table 3), this result was validated in analyses using

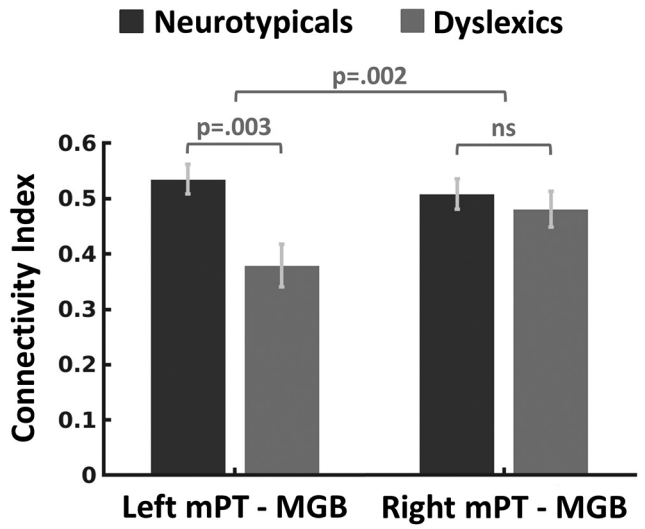

Figure 5. Mean connectivity strength for neurotypicals and dyslexics between the mPT and the MGB. Error bars indicate ± 1 SEM.

white matter ROIs (see "Functional localizer for ROI definition" section).

Is the white matter reduction between mPT and MGB specific to the left hemisphere?

We next tested whether dyslexics' reduction in mPT–MGB connectivity was specific to the left hemisphere. We assumed a specificity in connectivity reduction to the left hemisphere based on the findings that the left MGB showed atypical fMRI responses in dyslexics (Díaz et al., 2012) and that postmortem studies on brains of dyslexics found alterations in the left but not in the right MGB (Galaburda et al., 1994; cf. Stein, 2001). Also in the visual modality, the left-hemispheric cortico-thalamic connectivity was reduced in dyslexics compared with neurotypicals, whereas no equivalent effect emerged in the right hemisphere (Müller-Axt et al., 2017). We calculated a 2 × 2 mixed-effects ANOVA with the factors "hemisphere" (left vs right) and "group" (neurotypicals vs dyslexics) for ROIs containing both gray and white matter. Again, to control for potential biases due to volume size, these results were validated using ROIs that contained white matter volume proportions only (see "Functional localizer for ROI definition" section). The connection between right mPT and right MGB could be reliably estimated in all 24 participants. The ANOVA showed a significant hemisphere × group interaction ($F_{(1,21)} = 12.26$, $p = 0.002$, $\eta^2 = 0.369$; Fig. 5). *Post hoc t* tests revealed no significant difference in the right-hemispheric mPT–MGB connection between dyslexics and neurotypicals ($t_{(22)} = 0.647$, $p = 0.524$, $d = 0.264$; cf. Fig. 5), indicating that the interaction was driven by the significant group effect (dyslexics vs neurotypicals) in the connection between the left mPT and the left MGB ($t_{(21)} = 3.27$, $p = 0.003$, $d = 1.378$).

Is dyslexics' reduction in white matter connectivity specific to the left mPT–MGB connection, but not present in the A1–MGB connection?

When comparing the left mPT–MGB connection with the left A1–MGB connection, we expected no reduction in connectivity strength in the A1–MGB connection for two reasons: (1) human neuroimaging and postmortem brain analyses did not show any evidence of dyslexia related alterations in A1 (for review, see Eckert, 2004) and (2) there was no white matter connectivity reduction for dyslexics in the visual modality between V1 and the LGN (Müller-Axt et al., 2017). These two findings suggested that dyslexia-related structural alterations might not be reflected in cortico-thalamic connectivity involving primary sensory cortices.

The connection between A1 and MGB could be reliably estimated in all 24 participants in both hemispheres (Fig. 6). There was a marginally significant interaction in the 2 × 2 mixed-effects ANOVA with the factors "group" (neurotypicals vs dyslexics) and "seed region" (left A1 vs left mPT) with a medium effect size ($F_{(1,21)} = 3.71$, $p = 0.068$, $\eta^2 = 0.150$). In contrast to the left mPT–MGB connection (Figs. 4, 5), the connectivity strength of the left A1–MGB pathway was not significantly different between groups ($t_{(22)} = 1.49$, $p = 0.150$, $d = 0.608$). There was also no hemisphere × group interaction in the A1–MGB connection ($F_{(1,22)} = 1.08$, $p = 0.310$, $\eta^2 = 0.047$; Fig. 6).

Replication with ROIs that include white matter only

In addition to our analyses that included ROIs consisting of both gray and white matter, we replicated our hypothesis-driven analysis outcomes with ROIs that only contained white matter voxels. This was to control for potential biases due to differences in gray and white matter volume proportions across ROIs and to differences in overall ROI volume. There were no group effects in the size of left MGB volumes for ROIs that contained both gray and white matter (Table 2); however, we did observe a group difference in the size of the left mPT (Table 3). It is unlikely that this volume difference caused the group effect in left mPT–MGB connectivity strength because streamline counts in connectivity analyses were corrected for the size of the seed region; that is, the left mPT volume. Nevertheless, we aimed for replication of the group effect in left mPT–MGB connectivity strength with ROIs that did not show volume differences between groups.

Analyses with white matter ROIs revealed reliable tracking results in all participants ($N = 24$) and no group differences in the sizes of the left MGB volume (Table 2) or in the size of the left mPT mask (Table 3). Consistent with our first hypothesis, we again found weaker left mPT–MGB connectivity strength for dyslexics than neurotypicals ($t_{(21)} = 2.51$, $p = 0.019$, $d = 1.03$).

Further tests on the specificity of the mPT–MGB group effect showed qualitatively similar results as reported for the combined white and gray matter ROIs. There was a significant hemisphere × group interaction ($F_{(1,22)} = 7.10$, $p = 0.014$, $\eta^2 = 0.244$) driven by the reported group effect in left mPT–MGB connection, which was absent in the right hemisphere ($p = 0.982$). This was the case even though the white matter ROI of the right MGB was smaller in dyslexics than in neurotypicals. The results are consistent with analyses on masks that contained both gray and white matter voxels (Figs. 4, 5). White matter ROIs also did not reveal any significant group effect in the A1–MGB connection and the interaction from an 2 × 2 mixed-effects ANOVA with the factors "group" (neurotypicals vs dyslexics) and "seed region" (left A1 vs left mPT) was close to significance ($F_{(1,22)} = 4.24$, $p = 0.051$, $\eta^2 = 0.162$), similar to results for the combined white and gray matter ROIs (Fig. 6).

Control and exploratory analyses

Analysis of the left mPT–MGB connection via A1

We tested whether dyslexia related alterations in left mPT–MGB connectivity may originate from dysfunctional tracks that go via A1. Although there is evidence for direct cortico-thalamic con-

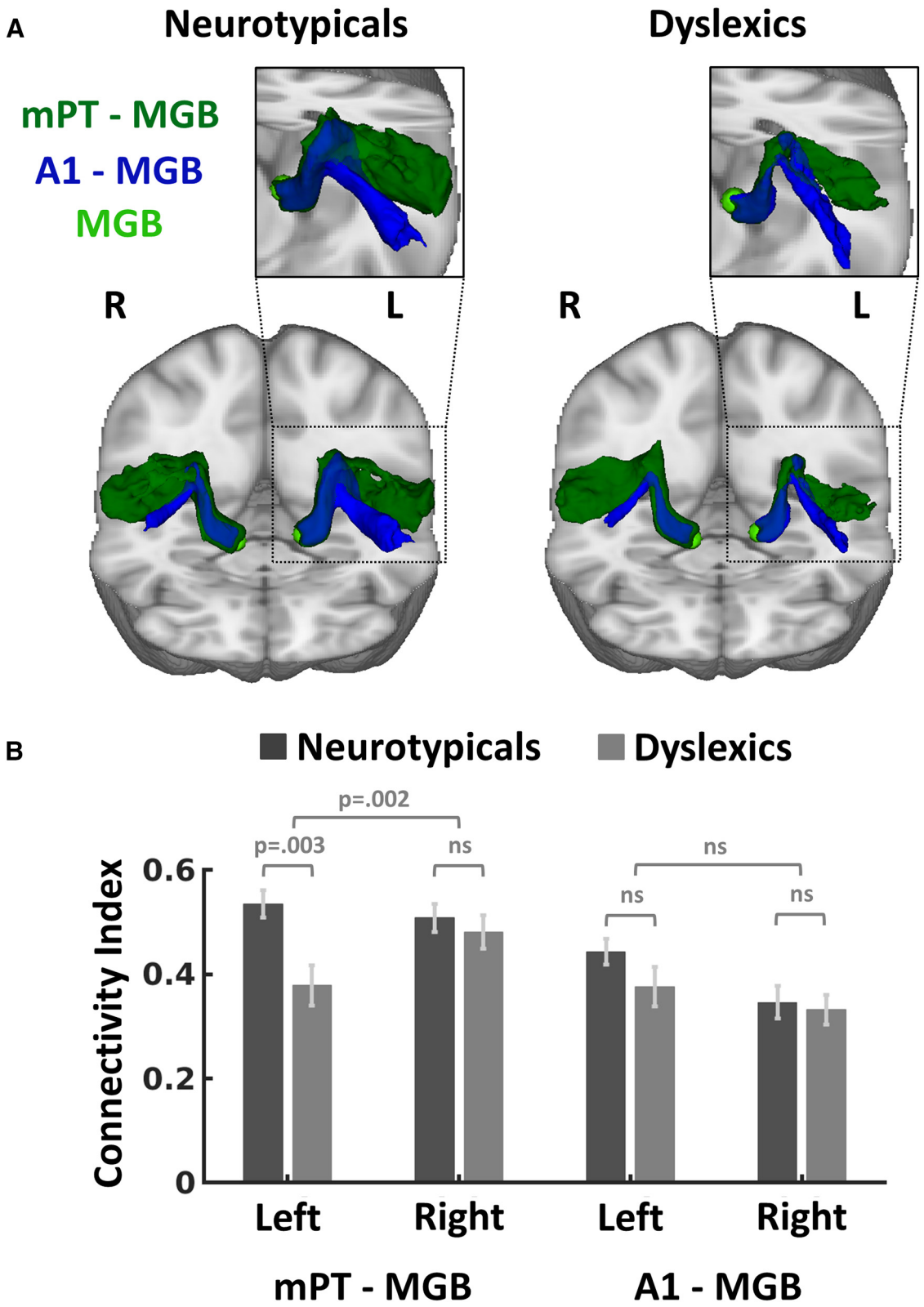

Figure 6. ***A***, Averaged probabilistic white matter connectivity for neurotypicals and dyslexics between the mPT and the MGB (dark green) and between A1 and the MGB (blue). The log-normalized and averaged tracks are presented in MNI standard space and thresholded to the same minimum value of 0.08. ***B***, Mean strength of the mPT–MGB and the A1–MGB connectivity for neurotypicals and dyslexics. Error bars indicate ± 1 SEM.

nectivity between higher-level auditory cortices such as the mPT and the MGB (Winer et al., 2001), it has been also suggested that some projections between the MGB and higher-level auditory cortices go via A1 (Rouiller et al., 1991; Lee, 2013). Therefore, we compared the left mPT–MGB track via A1 with the direct connection between the left mPT and left MGB.

For tractography analyses via A1, the left mPT was set as seed region, the left A1 as the waypoint, and the left MGB as the second

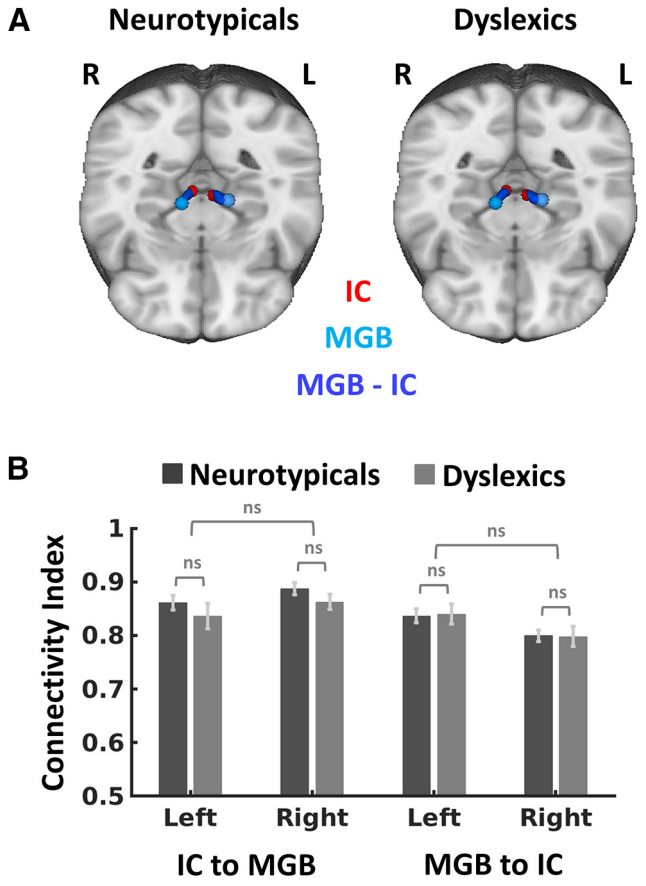

Figure 7. Averaged probabilistic white matter connectivity for neurotypicals and dyslexics between the MGB and the IC. ***A***, Log-normalized and averaged tracks are presented in MNI standard space and thresholded to the same minimum value of 0.50. ***B***, Mean connectivity strength of tracks between IC and MGB for neurotypicals and dyslexics. Error bars indicate ± 1 SEM.

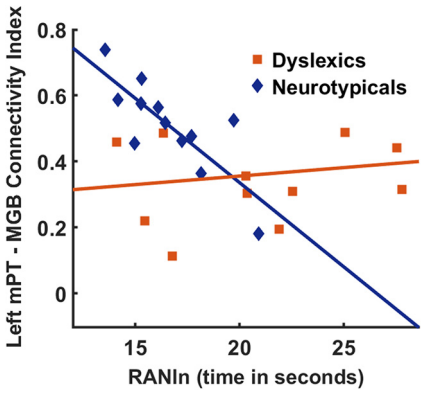

Figure 8. Correlation between the RANln and the connectivity index of the white matter pathway between the left mPT and the left MGB. A significantly negative correlation emerged for neurotypical participants, suggesting that stronger mPT–MGB connectivity was associated with faster RANln.

waypoint and termination mask. The tract via A1 showed overall weak connectivity strength compared with the direct left mPT–MGB connection: two neurotypicals and one dyslexic were excluded due to absence of reliable connections. We ran a 2 × 2 mixed-effects ANOVA with the factors "group" (neurotypicals vs dyslexics) and "track" (left mPT–MGB vs left mPT–MGB-via-A1) to assess whether group effects primarily emerged in the direct connection between left mPT and left MGB. A significant track × group interaction ($F_{(1,19)} = 6.28$, $p = 0.021$, $\eta^2 = 0.249$) showed dyslexics' reduction in connectivity strength in the direct left mPT–MGB connection ($t_{(21)} = 3.27$, $p = 0.003$, $d = 1.378$; Figs. 4, 5, 6), but not in the track via A1 ($t_{(21)} = 0.80$, $p = 0.427$, $d = 0.330$).

Analysis of MGB–IC connectivity

Several studies (Chandrasekaran et al., 2009; Chandrasekaran and Kraus, 2010) have associated dyslexia with alterations of auditory brainstem structures. We therefore explored group differences in the connectivity between the IC and the MGB, and ran independent tracking analyses for both directions (MGB-to-IC and IC-to-MGB) within each hemisphere. Connections between the IC and the MGB showed reliable tracking results, with at least 10 of the generated sample streamlines reaching the target mask for all participants (Fig. 7*A*). We analyzed group differences in the averaged IC-to-MGB and MGB-to-IC tracking results in the left hemisphere by means of a two-sample *t* test, as well as hemispheric differences in an ANOVA with the factors "hemisphere" (left vs right) and "group" (neurotypicals vs dyslexics). However, no main effect or interaction with the factors group or hemisphere emerged (all *p*-values >0.182; Fig. 7*B*). We obtained qualitatively similar results for the ROIs based on the alternative left IC coordinate (see Materials and Methods).

Correlation of left mPT–MGB connectivity strength with reading skills

Our second hypothesis was that lower scores in the RANln and in reading comprehension are accompanied by weaker connectivity strength between the left mPT and the left MGB in dyslexics. We focused on this connection because it showed reliable group differences between dyslexics and neurotypicals across our analyses, which is consistent with our hypothesis.

We Bonferroni corrected for the four conducted tests: the correlations between the two behavioral scores of interest, the RANln score, and the reading comprehension score and connectivity indices from analyses with ROIs containing gray and white matter voxels or white matter voxels only. Inconsistent with our hypotheses, there was no significant correlation between left mPT–MGB connectivity strength and the RANln score in dyslexics (all *p*-values >0.05). Dyslexics also did not show a significant correlation between left mPT–MGB connectivity strength and the reading comprehension score (all *p*-values >0.05); there was, however, a negative correlation of the RANln score with mPT–MGB connectivity strength in neurotypical readers for analyses with ROIs that contained white matter voxels only ($r = -0.798$, $p = 0.002$, 95% confidence interval: −0.310 to −0.979; Fig. 8). This indicates that stronger connectivity strength between left mPT and left MGB was associated with higher levels of reading fluency, as measured by faster rapid naming skills, in neurotypical readers. Despite a similar trend, no Bonferroni-corrected significant correlation was observed for analyses with ROIs containing both gray and white matter voxels ($r = -0.553$, $p = 0.077$).

Discussion

In the current study, we found three key results. First, there was a reduction in connectivity strength between the left mPT and the left MGB in dyslexics compared with neurotypical readers, consistent with our hypothesis. Second, dyslexics showed no reduction in structural connectivity in the right hemisphere or in any other analyzed section of the auditory pathway. Third, our hypothesis that connectivity strength between the left mPT and the

left MGB in dyslexics correlates with measures of reading fluency and reading comprehension was not confirmed. Instead, left mPT–MGB connectivity strength positively correlated with reading fluency in neurotypical readers. The results provide the first evidence for the long-standing hypothesis (Galaburda et al., 1994) that dyslexia related functional (Díaz et al., 2012) and structural (Galaburda et al., 1994; cf. Stein, 2001) alterations in subcortical regions of the auditory pathway (i.e., in the left MGB) are accompanied by reduced connectivity to specific higher-level auditory cortices.

The hypotheses for our study were based on the findings of two previous studies: an atypical task-dependent modulation of the left MGB was observed for dyslexics during a phonological task in contrast to a control task (Díaz et al., 2012) and dyslexics showed reduced connectivity between left V5/MT and the left LGN (Müller-Axt et al., 2017). The findings of the present study from the auditory modality mirror the previous findings in the visual modality (Müller-Axt et al., 2017). In that study, a reduction in the left-hemispheric pathway between the visual sensory thalamus (LGN) and the visual motion-sensitive cortex (MT/V5) was found in dyslexics compared with neurotypicals. In analogy, we here found a specific reduction in the left-hemispheric pathway between the MGB and the mPT in dyslexics compared with neurotypical readers. The results could not be explained by a general reduction in connectivity strength in dyslexia because there were no group differences in the right mPT–MGB pathway, the A1–MGB pathway, or the MGB–IC pathway. Left–right hemispheric asymmetries in the auditory modality have been found in other studies on the functional level (Belin et al., 1998; Schönwiesner et al., 2007) and the structural level (Mišic et al., 2018). In dyslexics, a specificity of the mPT–MGB pathway reduction to the left hemisphere is in agreement with its specialization for speech processing and the speech-perception-related deficits found in the dyslexia population such as phonological processing difficulties (Snowling and Melby-Lervåg, 2016).

The group difference in left mPT–MGB connectivity between dyslexics and neurotypicals reported here is large ($d = 1.37$) as was the effect size in the visual domain in the left V5/MT-to-LGN connection ($d = 1.28$) (Müller-Axt et al., 2017). Ramus et al. (2018) attempted to estimate the effect size of neuroanatomical differences in developmental disorders based on a voxel-based morphometry study in dyslexics (Eckert et al., 2016) and a meta-analysis of cortical thickness in subjects with autism spectrum disorder (Haar et al., 2016), concluding that effect sizes >0.5 in the field of dyslexia research might be inflated. However, whether the effects reported here observed in two sensory domains are inflated due to a modest sample size (Button et al., 2013) can only be answered by future (large-sample) DTI studies on developmental disorders.

Animal tracing studies detected independent fiber tracks between association auditory cortices and the MGB. Those studies discovered that the majority of neural fibers directly connect subnuclei of the MGB with different parts of the auditory association cortex (Hackett, 2011). Fiber-tracing analyses in cats revealed >12 independent connections from parts of the primary auditory cortex and from auditory association cortices to the MGB (Bajo et al., 1995; Winer et al., 2001). The homology of auditory cortex regions in animals and humans is a matter of debate (Zatorre and Belin, 2001) and it is therefore unclear which of the association auditory cortex regions that are directly connected to the MGB might correspond to the PT. However, because parts of the PT (Moerel et al., 2014; Saenz and Langers, 2014; Shrem and Deouell, 2014) are tonotopically organized in humans and direct fiber projections in both directions between all tonotopically organized regions and the MGB have been reported in animals (Bajo et al., 1995; Winer et al., 2001; Lee and Winer, 2008), it is likely that that direct fiber connections exist between the MGB and the PT in humans.

Evidence from animal models and human neuroimaging suggests that both the PT and MGB are sensitive to spectrotemporally complex sound. First, animal research on frequency modulated sweeps, which mimic the fast frequency modulations in speech, has shown that the ventral part of the MGB is especially sensitive to the direction of those sweeps; that is, changes from low to high frequencies and vice versa (Wenstrup, 1999; Lui and Mendelson, 2003). Second, a specific encoding of complex spectrotemporal characteristics in the PT has been shown in the context of auditory motion detection paradigms (for review, see Griffiths and Warren, 2002; Alink et al., 2012). Auditory and visual motion processing have been considered key components for the acquisition of reading and writing skills (Witton et al., 1998; Talcott et al., 2002; cf. Joo et al., 2017). Both types of motion processing were found to be deficient in children and adults with dyslexia (Stein, 2001; Amitay et al., 2002; Facoetti et al., 2003).

The visual and auditory motion processing cortices MT/V5 and mPT might modulate their corresponding sensory thalamic nuclei during the processing of spoken speech. Evidence for task-dependent modulation of sensory thalamic nuclei has been provided by means of fMRI: task-dependent modulation of the left MGB was stronger in a speech sound recognition task compared with a voice identity recognition task on the same stimuli (von Kriegstein et al., 2008; for similar findings on the LGN, see Díaz et al., 2018). This suggested that the MGB preferentially engages in the processing of phonological information compared with slowly occurring auditory features, such as required for voice identity detection. Developmental dyslexia has been associated with deficient task-dependent modulation of the left MGB specifically during phonological processing (Díaz et al., 2012). Therefore, our finding of reduced left mPT–MGB connectivity in dyslexics might reflect a reduction in cortico-thalamic feedback connections between mPT and MGB. However, this is speculative at present because probabilistic tracking analyses do not allow inferences on the direction of resolved connections.

Our analyses suggested that the left mPT–MGB connectivity may at least partially contribute to reading performance. This was supported by a significant correlation between lower reading fluency measures, as operationalized by the RANln, and weaker left mPT–MGB connectivity strength in neurotypical readers. The RANln has been linked to both the reading abilities of dyslexics (Semrud-Clikeman et al., 2000), as well as neurotypical readers (Miller et al., 2006). A meta-analysis with a sample size of >2000 found correlations between RANln and reading skills to be similarly strong in poor and neurotypical readers (Swanson et al., 2003). In the present study, correlation between RANln and left mPT–MGB connectivity strength was found only in neurotypical readers. Similar effects were previously reported for dyslexics: slower performance in the RANln was associated with weaker connection strength in the visual domain between left V5/MT and left LGN (Müller-Axt et al., 2017) and with reduced speech task-dependent modulation in the left MGB (Díaz et al., 2012). It is interesting that all studies reported an association of the respective neuroscience measures with RANln scores. However, it is unclear why two of the studies found associations in the dyslexia group and the present study only in the neurotypical group. Fur-

thermore, the results of the correlations in the present study have to be taken with caution because they did not correspond to our *a priori* hypothesis and were present only in one of the analyses (i.e., with white matter ROIs only).

We conclude that, for a comprehensive understanding of dyslexia mechanisms, cortico-thalamic structural alterations need to be taken into account. Specifically, the current study provided evidence for such alterations in the auditory system, whereas equivalent findings have been reported previously for the visual domain (Müller-Axt et al., 2017). This implies that developmental dyslexia needs to be discussed within a multisensory framework that also includes subcortical brain structures involved in earliest visual and auditory processing.

References

Alink A, Euler F, Kriegeskorte N, Singer W, Kohler A (2012) Auditory motion direction encoding in auditory cortex and high-level visual cortex. Hum Brain Mapp 33:969–978. CrossRef Medline

Altarelli I, Leroy F, Monzalvo K, Fluss J, Billard C, Dehaene-Lambertz G, Galaburda AM, Ramus F (2014) Planum temporale asymmetry in developmental dyslexia: revisiting an old question. Hum Brain Mapp 35: 5717–5735. CrossRef Medline

Amitay S, Ben-Yehudah G, Banai K, Ahissar M (2002) Disabled readers suffer from visual and auditory impairments but not from a specific magnocellular deficit. Brain 125:2272–2285. CrossRef Medline

Anwander A, Tittgemeyer M, von Cramon DY, Friederici AD, Knösche TR (2007) Connectivity-based parcellation of Broca's area. Cereb Cortex 17: 816–825. CrossRef Medline

Artacho-Pérula E, Arbizu J, Arroyo-Jimenez Mdel M, Marcos P, Martinez-Marcos A, Blaizot X, Insausti R (2004) Quantitative estimation of the primary auditory cortex in human brains. Brain Res 1008:20–28. CrossRef Medline

Bajo VM, Rouiller EM, Welker E, Clarke S, Villa AE, de Ribaupierre Y, de Ribaupierre F (1995) Morphology and spatial distribution of corticothalamic terminals originating from the cat auditory cortex. Hear Res 83:161–174. CrossRef Medline

Basser PJ, Pierpaoli C (1996) Microstructural and physiological features of tissues elucidated by quantitative-diffusion-tensor MRI. J Magn Reson B 111:209–219. CrossRef Medline

Basser PJ, Mattiello J, LeBihan D (1994) Estimation of the effective self-diffusion tensor from the NMR spin echo. J Magn Reson B 103:247–254. CrossRef Medline

Behrens TE, Johansen-Berg H (2005) Relating connectional architecture to grey matter function using diffusion imaging. Philos Trans R Soc Lond B Biol Sci 360:903–911. CrossRef Medline

Behrens TE, Woolrich MW, Jenkinson M, Johansen-Berg H, Nunes RG, Clare S, Matthews PM, Brady JM, Smith SM (2003) Characterization and propagation of uncertainty in diffusion-weighted MR imaging. Magn Reson Med 50:1077–1088. CrossRef Medline

Behrens TE, Berg HJ, Jbabdi S, Rushworth MF, Woolrich MW (2007) Probabilistic diffusion tractography with multiple fibre orientations: what can we gain? Neuroimage 34:144–155. CrossRef Medline

Belin P, Zilbovicius M, Crozier S, Thivard L, Fontaine A, Masure MC, Samson Y (1998) Lateralization of speech and auditory temporal processing. J Cogn Neurosci 10:536–540. CrossRef Medline

Blank H, Anwander A, von Kriegstein K (2011) Direct structural connections between voice- and face-recognition areas. J Neurosci 31:12906–12915. CrossRef Medline

Britten KH, Shadlen MN, Newsome WT, Movshon JA (1992) The analysis of visual motion: a comparison of neuronal and psychophysical performance. J Neurosci 12:4745–4765. CrossRef Medline

Button KS, Ioannidis JP, Mokrysz C, Nosek BA, Flint J, Robinson ES, Munafò MR (2013) Power failure: why small sample size undermines the reliability of neuroscience. Nat Rev Neurosci 14:365–376. CrossRef Medline

Carroll JM, Iles JE (2006) An assessment of anxiety levels in dyslexic students in higher education. Br J Educ Psychol 76:651–662. CrossRef Medline

Chandrasekaran B, Kraus N (2010) The scalp-recorded brainstem response to speech: neural origins and plasticity. Psychophysiology 47:236–246. CrossRef Medline

Chandrasekaran B, Hornickel J, Skoe E, Nicol T, Kraus N (2009) Context-dependent encoding in the human auditory brainstem relates to hearing speech in noise: implications for developmental dyslexia. Neuron 64:311–319. CrossRef Medline

Cohen J (1973) Eta-squared and partial eta-squared in fixed factor anova designs. Educational and Psychological Measurement 33:107–112. CrossRef

Cohen J (1988) Statistical power analysis for the behavioral sciences. Hillsdale, NJ: L. Erlbaum Associates.

De Martino F, Moerel M, van de Moortele PF, Ugurbil K, Goebel R, Yacoub E, Formisano E (2013) Spatial organization of frequency preference and selectivity in the human inferior colliculus. Nat Commun 4:1386. CrossRef Medline

Denckla MB, Rudel RG (1976) Rapid 'automatized' naming (R.A.N.): dyslexia differentiated from other learning disabilities. Neuropsychologia 14: 471–479. CrossRef Medline

Desikan RS, Ségonne F, Fischl B, Quinn BT, Dickerson BC, Blacker D, Buckner RL, Dale AM, Maguire RP, Hyman BT, Albert MS, Killiany RJ (2006) An automated labeling system for subdividing the human cerebral cortex on MRI scans into gyral based regions of interest. Neuroimage 31:968–980. CrossRef Medline

Devlin JT, Sillery EL, Hall DA, Hobden P, Behrens TE, Nunes RG, Clare S, Matthews PM, Moore DR, Johansen-Berg H (2006) Reliable identification of the auditory thalamus using multi-modal structural analyses. Neuroimage 30:1112–1120. CrossRef Medline

Díaz B, Hintz F, Kiebel SJ, von Kriegstein K (2012) Dysfunction of the auditory thalamus in developmental dyslexia. Proc Natl Acad Sci U S A 109:13841–13846. CrossRef Medline

Díaz B, Blank H, von Kriegstein K (2018) Task-dependent modulation of the visual sensory thalamus assists visual-speech recognition. Neuroimage 178:721–734. CrossRef Medline

Eckert M (2004) Neuroanatomical markers for dyslexia: a review of dyslexia structural imaging studies. Neuroscientist 10:362–371. CrossRef Medline

Eckert MA, Berninger VW, Vaden KI Jr, Gebregziabher M, Tsu L (2016) Gray matter features of reading disability: a combined meta-analytic and direct analysis approach. eNeuro 3:ENEURO.0103–0115.2015. CrossRef Medline

Eickhoff SB, Stephan KE, Mohlberg H, Grefkes C, Fink GR, Amunts K, Zilles K (2005) A new SPM toolbox for combining probabilistic cytoarchitectonic maps and functional imaging data. Neuroimage 25:1325–1335. CrossRef Medline

Facoetti A, Lorusso ML, Paganoni P, Cattaneo C, Galli R, Umiltà C, Mascetti GG (2003) Auditory and visual automatic attention deficits in developmental dyslexia. Brain Res Cogn Brain Res 16:185–191. CrossRef Medline

Galaburda AM, Sherman GF, Rosen GD, Aboitiz F, Geschwind N (1985) Developmental dyslexia: four consecutive patients with cortical anomalies. Ann Neurol 18:222–233. CrossRef Medline

Galaburda AM, Menard MT, Rosen GD (1994) Evidence for aberrant auditory anatomy in developmental dyslexia. Proc Natl Acad Sci U S A 91: 8010–8013. CrossRef Medline

Griffiths TD, Warren JD (2002) The planum temporale as a computational hub. Trends Neurosci 25:348–353. CrossRef Medline

Griswold MA, Jakob PM, Heidemann RM, Nittka M, Jellus V, Wang J, Kiefer B, Haase A (2002) Generalized autocalibrating partially parallel acquisitions (GRAPPA). Magn Reson Med 47:1202–1210. CrossRef Medline

Haar S, Berman S, Behrmann M, Dinstein I (2016) Anatomical abnormalities in autism? Cereb Cortex 26:1440–1452. CrossRef Medline

Hackett TA (2011) Information flow in the auditory cortical network. Hear Res 271:133–146. CrossRef Medline

Hall DA, Haggard MP, Akeroyd MA, Palmer AR, Summerfield AQ, Elliott MR, Gurney EM, Bowtell RW (1999) "sparse" temporal sampling in auditory fMRI. Hum Brain Mapp 7:213–223. CrossRef Medline

Heiervang E, Behrens TE, Mackay CE, Robson MD, Johansen-Berg H (2006) Between session reproducibility and between subject variability of diffusion MR and tractography measures. Neuroimage 33:867–877. CrossRef Medline

Hirayasu Y, McCarley RW, Salisbury DF, Tanaka S, Kwon JS, Frumin M, Snyderman D, Yurgelun-Todd D, Kikinis R, Jolesz FA, Shenton ME (2000) Planum temporale and heschl gyrus volume reduction in schizophrenia: a magnetic resonance imaging study of first-episode patients. Arch Gen Psychiatry 57:692–699. CrossRef Medline

Humphreys P, Kaufmann WE, Galaburda AM (1990) Developmental dyslexia in women: neuropathological findings in three patients. Ann Neurol 28:727–738. CrossRef Medline

Javad F, Warren JD, Micallef C, Thornton JS, Golay X, Yousry T, Mancini L (2014) Auditory tracts identified with combined fMRI and diffusion tractography. Neuroimage 84:562–574. CrossRef Medline

Jenkinson M, Bannister P, Brady M, Smith S (2002) Improved optimization for the robust and accurate linear registration and motion correction of brain images. Neuroimage 17:825–841. CrossRef Medline

Jiang F, Stecker GC, Fine I (2013) Functional localization of the auditory thalamus in individual human subjects. Neuroimage 78:295–304. CrossRef Medline

Jones DK (2010) Challenges and limitations of quantifying brain connectivity in vivo with diffusion MRI. Imaging in Medicine 2:341–355. CrossRef

Jones DK, Knösche TR, Turner R (2013) White matter integrity, fiber count, and other fallacies: the do's and don'ts of diffusion MRI. Neuroimage 73:239–254. CrossRef Medline

Joo SJ, Donnelly PM, Yeatman JD (2017) The causal relationship between dyslexia and motion perception reconsidered. Sci Rep 7:4185. CrossRef Medline

Kersting M, Althoff K (2004) RT-Rechtschreibungstest (3. Auflage). Göttingen, Germany: Hogrefe.

Langers DR (2014) Assessment of tonotopically organised subdivisions in human auditory cortex using volumetric and surface-based cortical alignments. Hum Brain Mapp 35:1544–1561. CrossRef Medline

Langers DR, van Dijk P (2012) Mapping the tonotopic organization in human auditory cortex with minimally salient acoustic stimulation. Cereb Cortex 22:2024–2038. CrossRef Medline

Lee CC (2013) Thalamic and cortical pathways supporting auditory processing. Brain Lang 126:22–28. CrossRef Medline

Lee CC, Winer JA (2008) Connections of cat auditory cortex: I. thalamocortical system. J Comp Neurol 507:1879–1900. CrossRef Medline

Lervåg A, Hulme C (2009) Rapid automatized naming (RAN) taps a mechanism that places constraints on the development of early reading fluency. Psychol Sci 20:1040–1048. CrossRef Medline

Lui B, Mendelson JR (2003) Frequency modulated sweep responses in the medial geniculate nucleus. Exp Brain Res 153:550–553. CrossRef Medline

Makuuchi M, Bahlmann J, Anwander A, Friederici AD (2009) Segregating the core computational faculty of human language from working memory. Proc Natl Acad Sci U S A 106:8362–8367. CrossRef Medline

Melcher JR, Sigalovsky IS, Guinan JJ Jr, Levine RA (2000) Lateralized tinnitus studied with functional magnetic resonance imaging: abnormal inferior colliculus activation. J Neurophysiol 83:1058–1072. CrossRef Medline

Miller CJ, Miller SR, Bloom JS, Jones L, Lindstrom W, Craggs J, Garcia-Barrera M, Semrud-Clikeman M, Gilger JW, Hynd GW (2006) Testing the double-deficit hypothesis in an adult sample. Ann Dyslexia 56:83–102. CrossRef Medline

Mišic B, Betzel RF, Griffa A, de Reus MA, He Y, Zuo X-N, van den Heuvel MP, Hagmann P, Sporns O, Zatorre RJ (2018) Network-based asymmetry of the human auditory system. Cereb Cortex 28:2655–2664. CrossRef Medline

Moerel M, De Martino F, Formisano E (2014) An anatomical and functional topography of human auditory cortical areas. Front Neurosci 8:225. CrossRef Medline

Moerel M, De Martino F, Uğurbil K, Yacoub E, Formisano E (2015) Processing of frequency and location in human subcortical auditory structures. Sci Rep 5:17048. CrossRef Medline

Müller-Axt C, Anwander A, von Kriegstein K (2017) Altered structural connectivity of the left visual thalamus in developmental dyslexia. Curr Biol 27:3692–3698.e3694. CrossRef Medline

Norton ES, Wolf M (2012) Rapid automatized naming (RAN) and reading fluency: implications for understanding and treatment of reading disabilities. Annu Rev Psychol 63:427–452. CrossRef Medline

Park HJ, Kubicki M, Westin CF, Talos IF, Brun A, Peiper S, Kikinis R, Jolesz FA, McCarley RW, Shenton ME (2004) Method for combining information from white matter fiber tracking and gray matter parcellation. AJNR Am J Neuroradiol 25:1318–1324. Medline

Peterson RL, Pennington BF (2012) Developmental dyslexia. Lancet 379:1997–2007. CrossRef Medline

Peterson RL, Pennington BF (2015) Developmental dyslexia. Annu Rev Clin Psychol 11:283–307. CrossRef Medline

Rademacher J, Morosan P, Schormann T, Schleicher A, Werner C, Freund HJ, Zilles K (2001) Probabilistic mapping and volume measurement of human primary auditory cortex. Neuroimage 13:669–683. CrossRef Medline

Rademacher J, Bürgel U, Zilles K (2002) Stereotaxic localization, intersubject variability, and interhemispheric differences of the human auditory thalamocortical system. Neuroimage 17:142–160. CrossRef Medline

Ramus F, Altarelli I, Jednoróg K, Zhao J, Scotto di Covella L (2018) Neuroanatomy of developmental dyslexia: pitfalls and promise. Neurosci Biobehav Rev 84:434–452. CrossRef Medline

Ratnanather JT, Poynton CB, Pisano DV, Crocker B, Postell E, Cebron S, Ceyhan E, Honeycutt NA, Mahon PB, Barta PE (2013) Morphometry of superior temporal gyrus and planum temporale in schizophrenia and psychotic bipolar disorder. Schizophr Res 150:476–483. CrossRef Medline

Raven JC (1998) Raven's progressive matrices. Oxford: Oxford Psychologists.

Ress D, Chandrasekaran B (2013) Tonotopic organization in the depth of human inferior colliculus. Front Hum Neurosci 7:586. CrossRef Medline

Rouiller EM, Simm GM, Villa AE, de Ribaupierre Y, de Ribaupierre F (1991) Auditory corticocortical interconnections in the cat: evidence for parallel and hierarchical arrangement of the auditory cortical areas. Exp Brain Res 86:483–505. CrossRef Medline

Royston P (1992) Approximating the Shapiro-Wilk W-test for non-normality. Statistics and Computing 2:117–119. CrossRef

Sabanciogullari V, Salk I, Balaban H, Oztoprak I, Kelkit S, Cimen M (2013) Magnetic resonance imaging mesencephalic tectum dimensions according to age and gender. Neurosciences (Riyadh) 18:33–39. Medline

Saenz M, Langers DR (2014) Tonotopic mapping of human auditory cortex. Hear Res 307:42–52. CrossRef Medline

Schneider W, Schlagmüller M, Ennemoser M (2007) Lesegeschwindigkeits- und -verständnistest für die Klassen, pp 6–12. Göttingen, Germany: Hogrefe.

Schönwiesner M, Krumbholz K, Rübsamen R, Fink GR, von Cramon DY (2007) Hemispheric asymmetry for auditory processing in the human auditory brain stem, thalamus, and cortex. Cereb Cortex 17:492–499. CrossRef Medline

Semrud-Clikeman M, Guy K, Griffin JD, Hynd GW (2000) Rapid naming deficits in children and adolescents with reading disabilities and attention deficit hyperactivity disorder. Brain Lang 74:70–83. CrossRef Medline

Shapleske J, Rossell SL, Woodruff PW, David AS (1999) The planum temporale: a systematic, quantitative review of its structural, functional and clinical significance. Brain Res Rev 29:26–49. CrossRef Medline

Shrem T, Deouell LY (2014) Frequency-dependent auditory space representation in the human planum temporale. Front Hum Neurosci 8:524. CrossRef Medline

Snowling MJ, Melby-Lervåg M (2016) Oral language deficits in familial dyslexia: a meta-analysis and review. Psychol Bull 142:498–545. CrossRef Medline

Soares JM, Marques P, Alves V, Sousa N (2013) A hitchhiker's guide to diffusion tensor imaging. Front Neurosci 7:31. CrossRef Medline

Stein J (2001) The magnocellular theory of developmental dyslexia. Dyslexia 7:12–36. CrossRef Medline

Swanson HL, Trainin G, Necoechea DM, Hammill DD (2003) Rapid naming, phonological awareness, and reading: a meta-analysis of the correlation evidence. Review of Educational Research 73:407–440. CrossRef

Talcott JB, Witton C, Hebb GS, Stoodley CJ, Westwood EA, France SJ, Hansen PC, Stein JF (2002) On the relationship between dynamic visual and auditory processing and literacy skills; results from a large primary-school study. Dyslexia 8:204–225. CrossRef Medline

Thomas C, Ye FQ, Irfanoglu MO, Modi P, Saleem KS, Leopold DA, Pierpaoli C (2014) Anatomical accuracy of brain connections derived from diffusion MRI tractography is inherently limited. Proc Natl Acad Sci U S A 111:16574–16579. CrossRef Medline

Thompson SK, von Kriegstein K, Deane-Pratt A, Marquardt T, Deichmann R, Griffiths TD, McAlpine D (2006) Representation of interaural time delay in the human auditory midbrain. Nat Neurosci 9:1096–1098. CrossRef Medline

Tourdias T, Saranathan M, Levesque IR, Su J, Rutt BK (2014) Visualization of intra-thalamic nuclei with optimized white-matter-nulled MPRAGE at 7T. Neuroimage 84:534–545. CrossRef Medline

Vandermosten M, Boets B, Wouters J, Ghesquière P (2012) A qualitative and quantitative review of diffusion tensor imaging studies in reading and dyslexia. Neurosci Biobehav Rev 36:1532–1552. CrossRef Medline

von Kriegstein K, Patterson RD, Griffiths TD (2008) Task-dependent modulation of medial geniculate body is behaviorally relevant for speech recognition. Curr Biol 18:1855–1859. CrossRef Medline

Warren JD, Zielinski BA, Green GG, Rauschecker JP, Griffiths TD (2002) Perception of sound-source motion by the human brain. Neuron 34:139–148. CrossRef Medline

Wenstrup JJ (1999) Frequency organization and responses to complex sounds in the medial geniculate body of the mustached bat. J Neurophysiol 82:2528–2544. CrossRef Medline

Westbury CF, Zatorre RJ, Evans AC (1999) Quantifying variability in the planum temporale: a probability map. Cereb Cortex 9:392–405. CrossRef Medline

Winer JA, Diehl JJ, Larue DT (2001) Projections of auditory cortex to the medial geniculate body of the cat. J Comp Neurol 430:27–55. CrossRef Medline

Witton C, Talcott JB, Hansen PC, Richardson AJ, Griffiths TD, Rees A, Stein JF, Green GG (1998) Sensitivity to dynamic auditory and visual stimuli predicts nonword reading ability in both dyslexic and normal readers. Curr Biol 8:791–797. CrossRef Medline

Zatorre RJ, Belin P (2001) Spectral and temporal processing in human auditory cortex. Cereb Cortex 11:946–953. CrossRef Medline

Zeki S (2015) Area V5: a microcosm of the visual brain. Front Integr Neurosci 9:21. CrossRef Medline